Magnetic inhomogeneity and variable-range hopping transport at temperatures above the ferromagnetic transition in $La_{1.4}Sr_{1.6}Mn_{2-y}Ti_yO_7$ system

Hong Zhu,[1] XianMing Liu,[2] KeQing Ruan,[3] and YuHeng Zhang[2]

[1]*Structure Research Laboratory and Department of Physics, University of Science and Technology of China, Hefei 230026, People's Republic of China*

[2]*Structure Research Laboratory, University of Science and Technology of China, National High Magnetic Field Laboratory, Hefei 230026, People's Republic of China*

[3]*Department of Physics, University of Science and Technology of China, Hefei 230026, People's Republic of China*

The magnetic and transport properties of the layered manganites $La_{1.4}Sr_{1.6}Mn_{2-y}Ti_yO_7$ ($y \leq 0.10$) are investigated. For the undoped and doped samples, magnetization and electron-spin-resonance experiments exhibit coexistence of the short-range ferromagnetic ordering and paramagnetic states at temperatures above the ferromagnetic transition. Meanwhile, the random potential in the systems increases with increasing Ti substitution. The magnetic inhomogeneities and random potential result in the Anderson localization. So the variable-range hopping processes dominate the transport behaviors at temperatures above the ferromagnetic transition in the $La_{1.4}Sr_{1.6}Mn_{2-y}Ti_yO_7$ ($y \leq 0.10$) systems.

I. INTRODUCTION

The colossal magnetoresistance (CMR) in rare-earth manganate perovskites $T_{1-x}D_xMnO_3$ (with T=La, Pr, Nd, Sm and D=Ca, Sr, Ba, Pb) is one of the most attractive subjects in recent years, both from the point of view of fundamental studies and potential applications.[1–6] Generally, the magnetic and transport properties of manganite oxides can be understood in terms of the double-exchange (DE) interaction[7,8] and the Jahn-Teller effects.[9] In addition, there are numerous reports on the magnetic-polaron formation caused by the spin-disorder scattering inherent to the DE model.[10–14] According to this scattering mechanism, the charge carriers moving in the slowly fluctuating spin background form magnetic polarons. Several authors also suggested a possible crucial role of the spin fluctuations on the resistivity and the CMR phenomena near and above T_C.[15,16] More recently, theoretical and experimental work is rapidly converging to a unified picture pointing toward a physics of manganites in the CMR materials clearly dominated by inhomogeneities in the form of coexisting competing phases.[17–19]

Besides in the ABO_3-type cubic perovskite manganites, the CMR effects also have been observed in $La_{2-2x}D_{1+2x}Mn_2O_7$ (D=Sr, Ca) with a tetragonal $Sr_3Ti_2O_7$-type layered perovskite structure.[20–24] As a layered perovskite, $La_{2-2x}D_{1+2x}Mn_2O_7$ (D=Sr, Ca) compound consists of the MnO_2 bilayers and rock-salt-type $(La,D)_2O_2$ layers. The MnO_2 bilayers are separated by rock-salt-type $(La,D)_2O_2$ layers along the c axis. Because of its structural anisotropy, it presents anisotropy of physical properties, including magnetic properties and transport behavior. It has been found that the magnetic coupling between Mn t_{2g} local spins in the MnO_2 bilayers is at least an order of magnitude stronger than that of interbilayers.[17] In addition, the layered manganites provide new interesting physics due to its quasi-two-dimensional character, such as enhanced fluctuation effects in the sense of reducing the Curie temperature T_C and

correspondingly enhanced magnetoresistance.[20,21] However, the importance of the magnetic fluctuations in the transport behavior has not been fully appreciated in the layered manganites.

We noticed that because the charge-carrier transport at temperatures above T_C is in a short-range two-dimensional (2D) ferromagnetic (FM) ordering background in the layered manganites $La_{2-2x}D_{1+2x}Mn_2O_7$ (D=Sr, Ca),[17] its conductive mechanism should be different from that of the ABO_3-type manganites. Moreover, element substitution at Mn sites would also cause random potential. We have reported the effects of Cu^{2+} substitution at Mn sites.[25] The results indicated that the Mn sites' substitution with Cu^{2+} ions changes the Mn^{3+}/Mn^{4+} proportion and the concentration of carriers. Here we select Ti^{4+} to substitute Mn^{4+} ions in the $La_{1.4}Sr_{1.6}Mn_{2-y}Ti_yO_7$ compounds for three reasons. First, the Ti^{4+} substitution keeps the lattice parameters unchanged because of the similar ion radius as $Mn^{3+/4+}$ ions. Second, Ti^{4+} substitution might increase the random potential in the systems. Third, the effects of Ti^{4+} substitution for Mn^{4+} ions on magnetic and transport properties should be more sensitive than the substitution of any other element for Mn^{3+}.

In the present paper, we report the results on the magnetic and transport behaviors in the double-layered $La_{1.4}Sr_{1.6}Mn_{2-y}Ti_yO_7$ ($y \leq 0.10$) perovskite compounds. It is indicated that the variable-range hopping (VRH) process dominates the transport behavior between T_C and room temperature in this system. The results are discussed in the framework of the Anderson localization model. We suggest that the magnetic inhomogeneities and random potential led to the VRH transport at temperatures above T_C in these layered manganites.

II. EXPERIMENTS

The bulk samples of $La_{1.4}Sr_{1.6}Mn_{2-y}Ti_yO_7$ (y=0.00, 0.02, 0.05, and 0.10) were synthesized by a standard ceramic
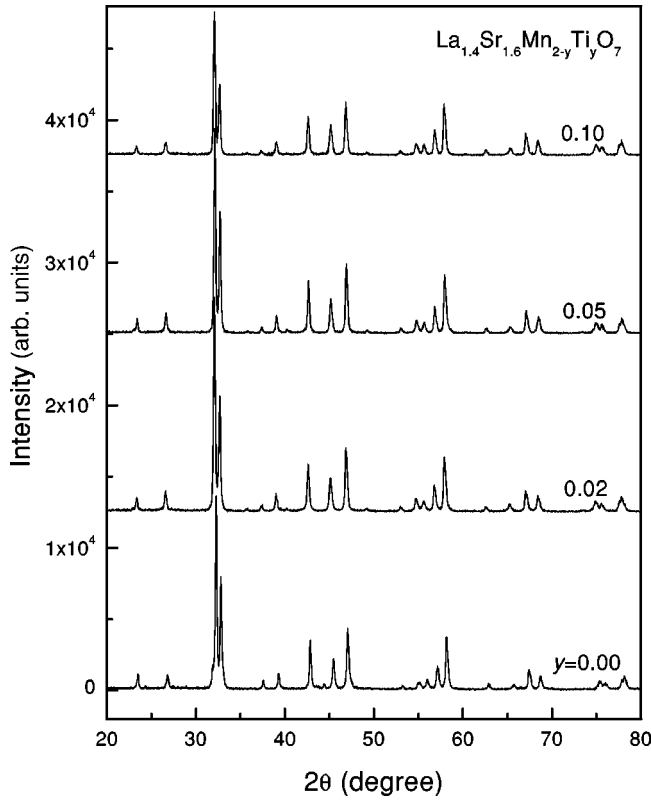
FIG. 1. X-ray diffraction patterns of samples $La_{1.4}Sr_{1.6}Mn_{2-y}Ti_yO_7$ ($y = 0.00, 0.02, 0.05, 0.10$).

FIG. 2. Temperature dependence of the low-field magnetization for samples $La_{1.4}Sr_{1.6}Mn_{2-y}Ti_yO_7$ ($y \leq 0.10$).

technique. The precursor materials were prepared by mixing stoichiometric amounts of La_2O_3, $SrCO_3$, MnO_2, and TiO_2. The powder was ground and calcined at $1100\,°C$ and $1350\,°C$ in air with intermediate grinding and then pressed into Φ10-mm plates, which were sintered at $1420\,°C$ for 20 h.

To characterize the samples, x-ray diffraction was carried out with a Rigaku D/Max-νA diffractometer operated with a graphite monochromator using Cu $K\alpha$ radiation ($\lambda = 0.1542$ nm). The electrical resistivity was measured by the standard four-point technique. The contacts are glued on a bar-shaped sample with silver-based epoxy. The temperature dependence of magnetization was measured by a VSM-9300 vibrating-sample magnetometer. The measurements were taken in both zero-field-cooled (ZFC) and field-cooled (FC) conditions under applied fields of 50 Oe. All the data were taken in the warming run. In order to investigate the specificity of the paramagnetic state and the short-range magnetic ordering, we observed the electron-spin-resonance (ESR) spectra. The ESR measurements were performed using a Bruker ER-200D-SRC spectrometer, operating at 9.47 GHz and between 100 K and 300 K.

III. EXPERIMENTAL RESULTS AND DISCUSSION

A. Structure of $La_{1.4}Sr_{1.6}Mn_{2-y}\,Ti_yO_7$ ($y \leq 0.10$) samples

The x-ray diffraction patterns for samples of $La_{1.4}Sr_{1.6}Mn_{2-y}Ti_yO_7$ ($y = 0.00, 0.02, 0.05$, and 0.10) are presented in Fig. 1. All the diffraction peaks are indexed with

respect to the $Sr_3Ti_2O_7$-type perovskite. The space is $I4/mmm$ with the lattice parameters of the tetragonal unit cell being $a = 0.3874$ nm and $c = 2.0082$ nm. Good agreement between the calculated and observed positions of the diffraction peaks indicates that the sample is a single phase of the $Sr_3Ti_2O_7$-type structure. By increasing the Ti doping level the positions of diffraction peaks do not change. This behavior is reasonable obviously, because the radius of Ti^{4+} (0.068 nm) is very close to that of Mn^{3+} (0.066 nm) and Mn^{4+} (0.060 nm).

B. Ti doping effects on magnetic and transport properties

The temperature dependence of magnetization for $La_{1.4}Sr_{1.6}Mn_{2-y}Ti_yO_7$ ($y \leq 0.10$) measured at a field of 50 Oe is presented in Fig. 2. For undoped and lightly Ti-doped samples ($x = 0.02, 0.05$), the ZFC and FC magnetizations increase sharply below $T_C \sim 90$ K, which is a signature of the 3D FM transition. For an undoped sample, the order of saturation magnetization $M_s \sim 10^1$ emu/g is the same as the ferromagnetically ordered $Pr_{1-x}Ca_xMnO_3$,[26] which indicates that the low-temperature phase is FM. Referring to the results of the neutron-diffraction experiments,[17] a visible plateau between 90 K and 350 K indicates that short-range 2D FM ordering occurs in this temperature range. That the magnetization decreases to zero around ~ 350 K marks a transition from a magnetic ordering to a paramagnetic (PM) state.

It can be seen that the temperature dependence of ZFC and FC magnetizations below $T_N \sim 45$ K is quite different. The ZFC magnetization decreases anomalously with further decreasing temperature. However, the FC magnetization does not exhibit this behavior. It increases with lowering temperature and tends towards saturation.

The neutron-scattering experiments have reported different magnetic structures at low temperature for La$_{1.4}$Sr$_{1.6}$Mn$_2$O$_7$ compounds. Perring et al.[27] proposed a low-temperature interbilayer antiferromagnetic (AFM) structure accompanying an intrabilayer FM with the easy axis parallel to the c axis. Argyriou et al.[28] reported the coexistence of the majority phase with a tilted AFM structure and the minority phase with a tilted FM structure in their $x = 0.3$ compound. The tilt angle, which is defined as an angle between the magnetic moment and the c axis, approaches $0°$ as the temperature decreases for both phases. M. Kubota et al.[29,30] reported the uniaxial FM phase at low temperature in their $x = 0.3$ sample. A more detailed study on a sufficiently homogeneous sample with precisely actual hole concentration is required to completely clarify the magnetic structure. But it is clear that the competition between the interbilayer FM and AFM magnetic couplings is quite strong around $x = 0.3$. In conjunction with the neutron-scattering data, the decrease of the ZFC magnetization at low temperature means that the interbilayer-canted AFM ordering takes place at T_N. The canting decreases with decreasing temperature and the magnetic moments align along the c axis at low temperatures. The evolution of interbilayer AFM ordering below T_N causes the decrease of magnetization at the ZFC condition. At temperatures below T_C, the different temperature dependence between M_{ZFC} and M_{FC} is quite similar to a spin-glass-like behavior. We noticed that the competition between the interbilayer FM and AFM magnetic couplings is quite strong in $x=0.3$ systems. So this spin-glass-like behavior is understandable. At FC condition, the magnetic moments become frozen in with decreasing temperature and the magnetization at the low temperatures does not decrease. For higher-Ti-content composition ($y = 0.05$), the 3D FM transition position shifts to a lower temperature and the magnetization decreases sharply. As Ti doping level in the sample increases further, magnetization of a heavily doped sample ($y = 0.10$) does not show any sign of 3D FM ordering down to 5 K and decreases further in the entire temperature range as displayed in Fig. 2(b). These results show that Ti substitution suppresses 3D FM ordering quickly. The short-range 2D FM ordering is also suppressed by Ti doping, but it remains in a heavily Ti-doped sample.

Figure 3 shows the temperature dependence of electrical resistivity ρ for La$_{1.4}$Sr$_{1.6}$Mn$_{2-y}$Ti$_y$O$_7$ ($y \leq 0.10$) samples. A peak near $T_{max}^{\rho} \sim 80$ K in the ρ-T curves indicates that the undoped and lightly doped samples ($y \leq 0.02$) undergo a metal-insulator (MI) transition. At temperatures above T_{max}^{ρ} the temperature dependence of resistivity presents a semiconductorlike behavior ($d\rho/dT < 0$), and at that below it, presents a metal-like behavior ($d\rho/dT > 0$). From M-T and ρ-T curves, it can be seen that the onset of 3D FM ordering is accompanied by the transport-property transition to metal-
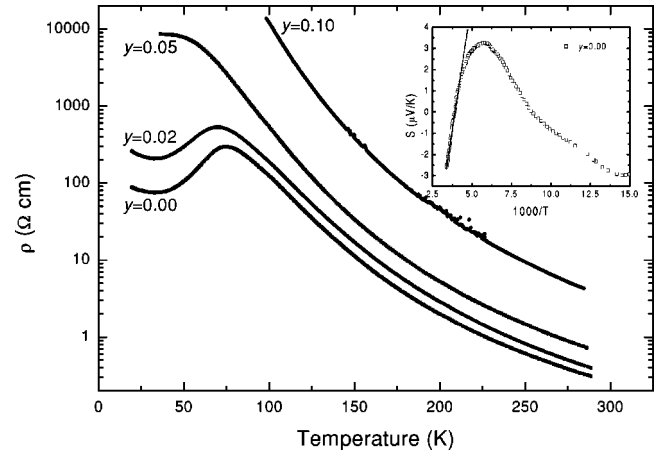
FIG. 3. Temperature dependence of the electrical resistivity for samples La$_{1.4}$Sr$_{1.6}$Mn$_{2-y}$Ti$_y$O$_7$ ($y \leq 0.10$). Inset: The Seebeck coefficient S for an undoped sample ($y=0.00$) shown as a function of inverse temperature.

lic behavior. Below T_C, it is interesting that a marked minimum appears in the ρ-T curves at a temperature of about 30 K. As mentioned above in the magnetization measurement, the interbilayer-canted AFM takes place at T_N and the canting decreases with lowering temperature. The anomalous transition to the semiconductorlike state below 30 K seems to be attributed to the increase of AFM ordering with magnetic moments aligning along the c axis. By increasing the Ti doping level, the resistivity increases and T_{max}^{ρ} shifts to the low-temperature side. For a $y = 0.05$ sample, an MI transition is displayed as an inflection point in our measuring range. By further increasing the doping level y, the resistivity of a heavily doped sample ($y = 0.10$) increases dramatically and the MI transition disappears. This reflects the results of suppression of the FM-PM transition by Ti doping. It is clear that replacing Mn by Ti hampers the electron transfer through the Mn^{3+}-O^{2-}-Mn^{4+} network seriously.

From the experimental results mentioned above, it can be seen that Ti substitution for Mn causes an increase of electrical resistivity and the disappearance of the I-M transition. With increasing Ti concentration, the 3D ferromagnetic transition disappears gradually. This behavior is common in the effects of Mn-site substitution in $T_{1-x}D_x$MnO$_3$ CMR compounds, similar to our results of Cu substitution for Mn in the La$_{1.4}$Sr$_{1.6}$Mn$_2$O$_7$ compound published previously.[25] But the effects of Ti substitution for Mn are more obvious than those of Cu substitution. As seen in Fig. 2, the low-field M with Ti doping level $y = 0.10$ is less than 0.5 emu/g. But for a Cu-doped sample with $y = 0.10$, the low-field M is nearly 1.5 emu/g. We consider that it is mainly due to the valency difference between the Cu^{2+} and Ti^{4+} ions. As Cu^{2+} is substituted for Mn, the amount of Mn^{4+} increases for valent equilibrium. Whereas for Ti^{4+} substitution for Mn, the amount of Mn^{4+} decreases. As is well known, the Mn^{4+} ions provide vacancies in the doped manganites. So reduction of the Mn^{4+} ions badly suppress the DE exchange between mixed-valent Mn ions.
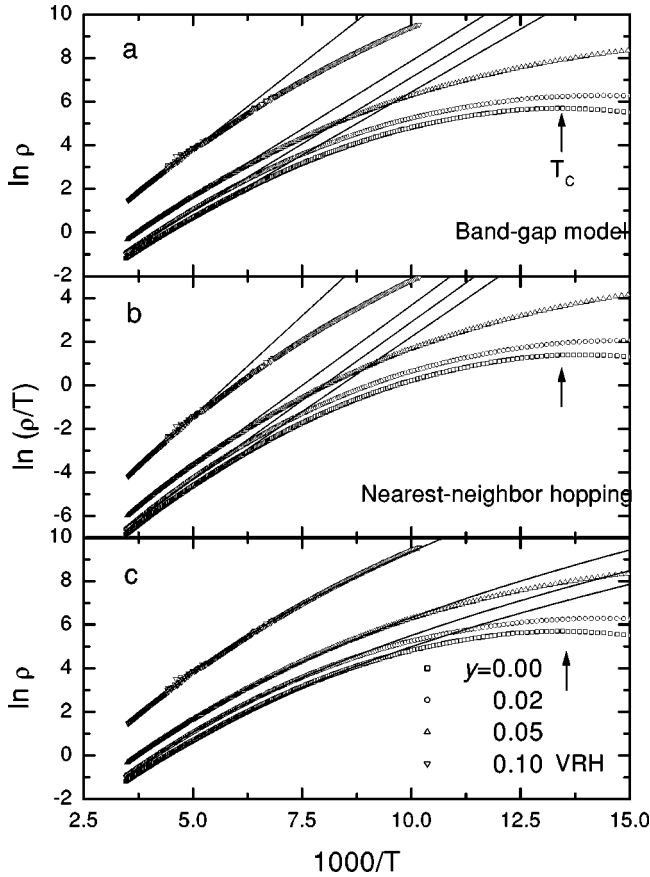
FIG. 4. $\ln(\rho)$ and $\ln(\rho/T)$ shown as a function of inverse temperature for samples $La_{1.4}Sr_{1.6}Mn_{2-y}Ti_yO_7$. The band-gap (a) and nearest-neighbor hopping (b) models (solid lines) fit the data in a narrow temperature range ($T > 150$ K). The variable-range hopping (c) model (solid line) fits the data in a wider temperature range ($T > 100$ K).

C. Variable-range hopping transport in layered manganites $La_{1.4}Sr_{1.6}Mn_{2-y}Ti_yO_7$

The semiconductorlike behavior of resistivity at temperatures above T^ρ_{max} are generally discussed in three models, i.e., a band-gap model,[31] a nearest-neighbor hopping model for the transport of small polarons,[32] and a VRH model.[33] An Arrhenius law $\rho = \rho_\infty \exp(E_\rho/k_BT)$ is used to thermally activate a process due to a band gap or a mobility edge. In the nearest-neighbor hopping model, the resistivity of the sample is given by $\rho = AT \exp(W_p/k_BT)$ with $W_p = E_p/2 - t$. E_p denotes the polaron-formation energy and t the electronic-

transfer integral. In Mott's VRH model, the resistivity is expressed in the form of $\rho = \rho_\infty \exp[(T_0/T)^{1/4}]$.

In order to clarify the transport mechanism at temperatures above T_C, we use our experimental data to check the three models mentioned above. Figure 4 displays the fitting results of the different models. The points are experimental data and the solid lines are the theoretic curves of the models. The fitting parameters E_ρ, W_p, T_0 and the valid temperature ranges are given in Table I. It can be seen in Fig. 4(a) that the Arrhenius law can fit the data at high temperatures above 170 K, and $E_\rho = 200$ meV is given as a fitting parameter in Table I. We also measured the temperature dependence of the thermoelectric power for an undoped sample. The thermopower experimental result presented in the inset of Fig. 3 shows that the Seebeck coefficient follows a thermally activated behavior[34] $S = (k/e)(E_S/k_BT) + S_\infty$ at high temperatures. But the activation energy $E_s = 5.0$ meV derived from thermopower data is much smaller than the activation energy E_ρ derived from the resistivity measurement. This difference is inconsistent with the band-gap model.[35] So we discard the action of a gap semiconductor or mobility edge as unlikely.

Figures 4(b) and 4(c) display the fitting results using the nearest-neighbor hopping model and the VRH model, respectively. It can be seen in the fitting parameters presented in Table I that the nearest-neighbor hopping model fits the data only in a limited temperature region far above T_C, whereas the VRH model gives a satisfactory fit in a wide temperature region above T_C. This led us to conclude that the VRH process dominates the conduction mechanism above T_C in these layered manganites.

Some authors have shown that the nearest-neighbor hopping model of small polarons best describes the intrinsic resistivity of cubic manganite $T_{1-x}D_xMnO_3$ in the PM states, and the activated energy of small polarons increases greatly with Mn-site doping. But from our resistivity data, we noticed that the ρ-T curves of the samples with different Ti-doping levels are almost parallel to each other at high temperatures and the activated energies do not change greatly. This behavior indicates that the VRH process is reasonable in the layered manganites $La_{2-2x}D_{1+2x}Mn_2O_7$ at temperatures above T_C.

If Anderson localization is taken into account in attempts to explain the transport properties in the layered manganites, the carrier transport is a hopping process between the localized states. According to the localization-state transport theory,[35] the hopping probability of localized carriers can be

TABLE I. Fitting parameters and valid temperature ranges of the various samples for the band-gap, nearest-neighbor hopping (NNH), and the variable-range hopping (VRH) model.

	Band gap		NNH		VRH	
y	T range (K)	E_ρ (meV)	T range (K)	W_p (meV)	T range (K)	T_0 (10^6 K)
0.00	>150	200	>150	118	>100	51.5
0.02	>150	210	>150	124	>100	60.0
0.05	>150	215	>150	127	>90	71.4
0.10	>180	270	>180	159	>90	146.4
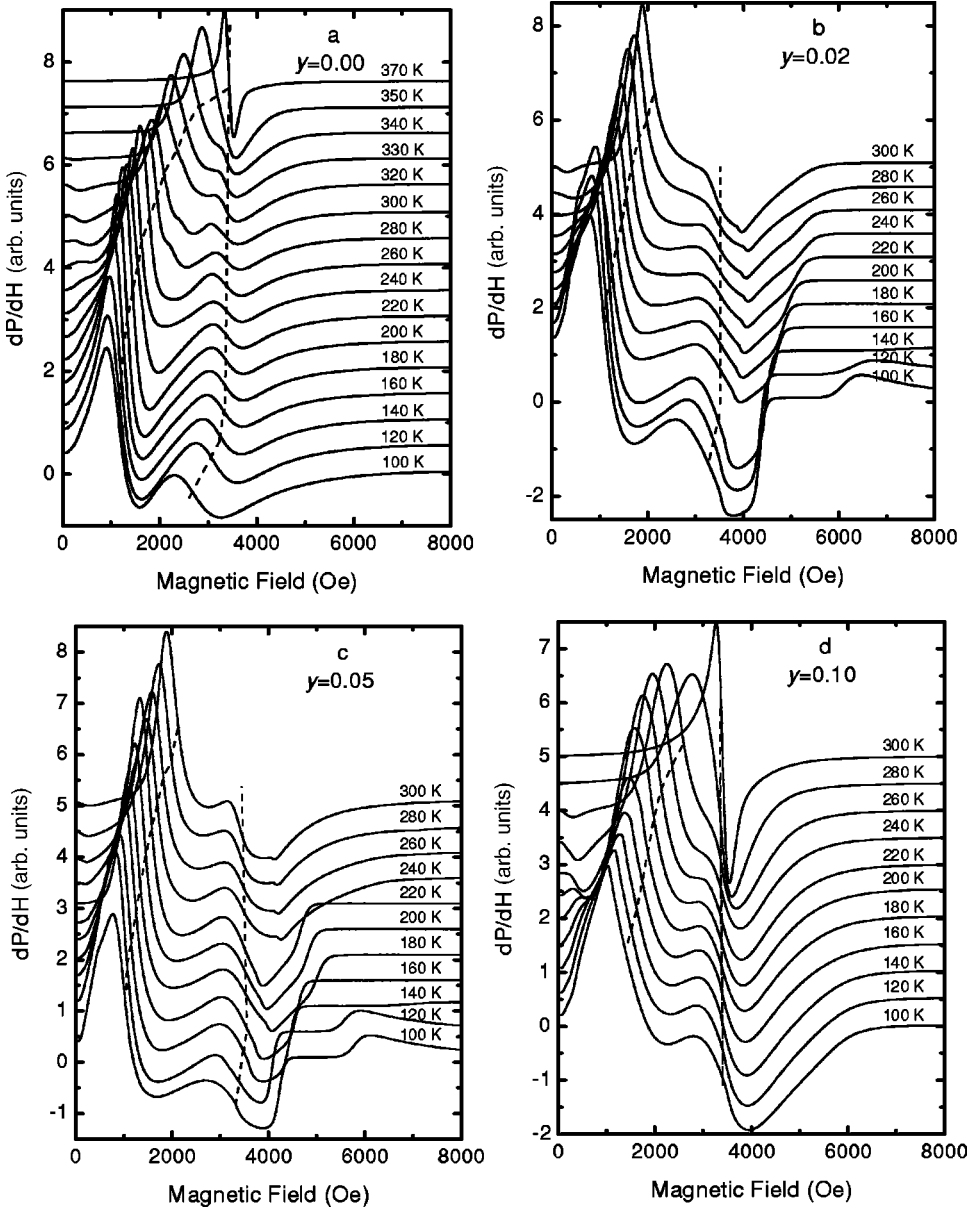
expressed as $\nu_{ph}\exp(-2\alpha R_0)\exp(-\triangle W/k_B T)$. Here, ν_{ph} is the thermal-vibration frequency of the phonon, $1/\alpha$ and R_0 denote the localization length and the average distance of the nearest localized state, respectively, $\exp(-\triangle W/k_B T)$ is a Boltzmann factor due to the energy difference $\triangle W$ between the two localized states. The dominant hopping mechanism could be either nearest neighbor or variable range depending mostly on the relation between the localization length $1/\alpha$ and the average distance R_0 of the nearest localized state. When $R_0 \gg 1/\alpha$, the conduction is favorable for the nearest-neighbor hopping process. When $R_0 \leqslant 1/\alpha$, it is favorable for the VRH process.

In the VRH model, $\rho = \rho_\infty \exp[(T_0/T)^{1/4}]$, the characteristic temperature T_0 depends on the localization length $1/\alpha$, which is described by[36] $T_0 = 24\alpha^3/\pi g_{(E_F)}k_B$, $g_{(E_F)}$ denotes the density of states at the Fermi level. Using the electronic density of states $g_{(E_F)}$ from low-temperature heat-capacity measurements[37] as 10^{22}/eV cm^3 and the fitting parameter T_0

presented in Table I, we deduced that the localization length $1/\alpha \sim 10^{-10}$ m. We assume that the average distance of the nearest localized state R_0 is of the same order as the distance between neighboring Mn sites $\sim 10^{-10}$ m. So the condition for VRH transport, $R_0 \leqslant 1/\alpha$, can be met in the layered manganites.

D. Magnetic inhomogeneity and random potential— the background for variable-range hopping transport

As we know, the magnetic inhomogeneities and random potential play an important role in the localized states. In order to investigate the specificity of the short-range magnetic-ordering states in the temperature range above $T_C \sim 90$ K, we measured the ESR spectra for different doped samples. As shown in Fig. 5, only a symmetrical absorption with $g \sim 2.0$ is presented at high temperature $T = 370$ K for an undoped sample ($y = 0.00$). This PM absorption is attributed to the spins without magnetic coupling between them.

This result is consistent with the PM state of the sample. As $T < 370$ K, the asymmetric, complex signals are observed in the differential spectra $dP/dH - H$. There are two kinds of ESR signals, i.e., the low-field absorption with g value much greater than 2.0 and the high-field absorption with g value very close to 2.0 in the temperature region above T_C ~ 90 K. This is in contrast with the pseudocubic manganite perovskites $T_{1-x}D_x MnO_3$, where only one PM ESR line with $g \sim 2.0$ is presented for $T > T_C$. Referring to our M-T results, the low-field line ($g > 2.0$) is attributed to the 2D short-range FM ordering and the high-field line ($g \sim 2.0$) is attributed to the paramagnetic state. With decreasing temperature, the low-field line shifts to a lower field, which means enhancement of FM coupling in the clusters. As the temperature is lowered to T_C, the PM line of an undoped sample begins shifting to the lower field obviously. As $T = 100$ K, disappearance of the PM line in the ESR spectra presented in Fig. 5(a) indicates that the system enters the FM state entirely. It is consistent with the 3D FM transition as presented in the M-T curves. As presented in Figs. 2, 5(b), and 5(c), the ESR lines of the doped samples ($y = 0.02, 0.05$) at lower temperatures are similar to that of an undoped sample. From the above discussion, it can be seen that the coexistence of short-range FM ordering and PM state causes magnetic inhomogeneities in the temperature region above T_C. The inhomogeneities and fluctuation effects of the magnetic structure cause the electronic densities of localized states to increase greatly in the layered manganites $La_{2-2x}D_{1+2x}Mn_2O_7$. The average distance of the nearest localized state R_0 decreases greatly to smaller than the localization length $1/\alpha$. So it is understandable that the VRH process is an intrinsic transport mechanism in the layered manganites.

By increasing the Ti doping level to $y = 0.10$, the magnetic ordering in MnO layers is destroyed quickly and the 3D FM transition disappears. The short-range 2D FM ordering in a heavily doped sample remains as at low temperatures, as presented in the M-T curve for $y = 0.10$ sample (Fig. 2). It can be seen in the ESR spectra that for a heavily Ti-doped sample ($y = 0.10$), a single, symmetrical PM absorption peak appears at temperatures above 280 K, which is much lower than that for an undoped sample (370 K). As presented in Fig. 5(d), the low-field absorption peaks corresponding to the short-range 2D FM ordering shift towards the PM absorption position. The g value (~ 6.18) of low-field lines at 100 K for undoped and doped samples ($y \leq 0.05$) remains unchanged. But when y increases to 0.10, the low-field g value at 100 K decreases to 4.53. It means weakening of the short-range 2D FM coupling. It also can be seen that the positions of the PM lines remain unchanged as the temperature is lowered from 300 K to 100 K. From these ESR experimental results, we can conclude that the Ti substitution at Mn sites decreases the magnetic coupling and the inhomogeneities at temperatures above T_C. So that the background for VRH transport should be weakened in a heavily doped sample. But as mentioned above, the VRH model also fits the resistivity data quite well for the $y = 0.10$ sample. We consider that enhancement of the random potential caused by Ti doping also plays an important role in the VRH transport for a highly doped sample. It is well known that the electronic configurations of Mn^{3+} and Mn^{4+} are $[Ar]t_{2g}^3 e_g^1$ and $[Ar]t_{2g}^3 e_g^0$, respectively, with different local Coulomb potentials. When Ti^{4+} ions with $[Ar]t_{2g}^0 e_g^0$ electronic configuration substitute for Mn ions, its Coulomb potential is quite different from that of Mn ions. Ti^{4+} random substitution at Mn sites must increase the random potential in the systems. Meanwhile, the density of localized states increases greatly with the increase in Ti^{4+} doping level. So the heavily doped samples provide a strong random-potential background for VRH transport.

In summary, the VRH transport at temperatures above T_C is due to the magnetic inhomogeneities and enhancement of random potential in the $La_{1.4}Sr_{1.6}Mn_{2-y}Ti_yO_7$ ($y \leq 0.10$) systems.

IV. CONCLUSIONS

In $La_{1.4}Sr_{1.6}Mn_{2-y}Ti_yO_7$ ($y \leq 0.10$) samples, we found that the ρ-T curves at temperatures above T_C are almost parallel to each other with increasing Ti substitution. It is different from the semiconductorlike behavior; with increasing doping level in $T_{1-x}D_x MnO_3$, the resistivity increases more and more sharply on lowering the temperature. All the curves are fitted quite well in the VRH mechanism. The rationality of the VRH mechanism in this system is discussed in terms of the Anderson localization transport theory. The macroscopic magnetization and microscopic ESR experimental results suggest that the coexistence of 2D short-range FM and PM states causes magnetic inhomogeneities in the temperature range between T_C and 350 K. The introduction of a random potential due to Ti^{4+} substitution is discussed in the electronic configuration of Ti ions. The magnetic inhomogeneities and random potential cause the background for the VRH transport of carriers. We suggest that the VRH transport at temperatures above T_C is reasonable in the $La_{1.4}Sr_{1.6}Mn_{2-y}Ti_yO_7$ system.

[1] A. Urushibara, Y. Moritomo, T. Arima, A. Asamitsu, G. Kido, and Y. Tokura, Phys. Rev. B **51**, 14 103 (1995).

[2] P. Schiffer, A. P. Ramirez, W. Bao, and S.-W. Cheong, Phys. Rev. Lett. **75**, 3336 (1995).

[3] P. G. Radaelli, M. Marezio, H. Y. Hwang, S.-W. Cheong, and B. Batlogg, Phys. Rev. B **54**, 8992 (1996).

[4] Y. Moritomo, A. Asamitsu, and Y. Tokura, Phys. Rev. B **56**, 12 190 (1997).

[5] J. F. Mitchell, D. N. Argyriou, J. D. Jorgensen, D. G. Hinks, C. D. Potter, and S. D. Bader, Phys. Rev. B **55**, 63 (1997).

[6] J. M. De Teresa, M. R. Ibarra, J. Blasco, J. Garcia, C. Marquina, P. A. Algarabel, Z. Arnold, K. Kamenev, C. Ritter, and R. Von Helmholt, Phys. Rev. B **54**, 1187 (1996).

[7] C. Zener, Phys. Rev. **82**, 403 (1951).

[8] P. W. Anderson and H. Hasegawa, Phys. Rev. **100**, 675 (1955).

[9] A. J. Millis, P. B. Littlewood, and B. I. Shraiman, Phys. Rev. Lett. **74**, 5144 (1995).

[10] C. M. Varma, Phys. Rev. B **54**, 7328 (1996).

[11] P. Horsch, J. Jaklic, and F. Mack, Phys. Rev. B **59**, R14 149 (1999).

[12] C. D. Batista, J. Eroles, M. Avignon, and B. Alascio, Phys. Rev. B **58**, R14 689 (1998).

[13] H. Yi and S. Lee, Phys. Rev. B **60**, 6250 (1999); H. Yi, J. Yu, and S. Lee, *ibid.* **61**, 428 (2000).

[14] W. S. Liu, Y. Chen, S. J. Xiong, and D. Y. Xing, Phys. Rev. B **60**, 5295 (1999).

[15] N. Furukawa, J. Phys. Soc. Jpn. **63**, 3214 (1994); **64**, 3164 (1995).

[16] S. Ishizaka and S. Ishihara, Phys. Rev. B **59**, 8375 (1999).

[17] T. G. Perring, G. Aeppli, Y. Moritomo, and Y. Tokura, Phys. Rev. Lett. **78**, 3197 (1997).

[18] D. N. Argyriou, H. N. Bordallo, B. J. Campbell, A. K. Cheetham, D. E. Cox, J. S. Gardner, K. Hanif, A. dos Santos, and G. F. Strouse, Phys. Rev. B **61**, 15 269 (2000).

[19] M. Mayr, A. Moreo, J. A. Verges, J. Arispe, A. Feiguin, and E. Dagotto, Phys. Rev. Lett. **86**, 135 (2001).

[20] Y. Moritomo, Y. Tomioka, A. Asamitsu, Y. Tokura, and Y. Matsui, Nature (London) **380**, 141 (1996).

[21] T. Kimura, Y. Tomioka, H. Kuwahara, A. Asamitsu, M. Tamura, and Y. Tokura, Science **274**, 1698 (1996).

[22] H. Asano, J. Hayakawa, and M. Matsui, Appl. Phys. Lett. **68**, 3638 (1996).

[23] D. N. Argyriou, J. F. Mitchell, C. D. Potter, S. D. Bader, R. Kleb, and J.-D. Jorgensen, Phys. Rev. B **55**, R11 965 (1997).

[24] R. Seshadri, A. Maignan, M. Hervieu, N. Nguyen, and B. Raveau, Solid State Commun. **101**, 453 (1997).

[25] H. Zhu, X. J. Xu, L. Pi, and Y. H. Zhang, Phys. Rev. B **62**, 6754 (2000).

[26] M. R. Lees, J. Barratt, G. Balakrishnan, D. Mck. Paul, and C. D. Dewhurst, J. Phys.: Condens. Matter **8**, 2967 (1996).

[27] T. G. Perring, G. Aeppli, T. Kimura, Y. Tokura, and M. A. Adams, Phys. Rev. B **58**, R14 693 (1998).

[28] D. N. Argyriou, J. F. Mitchell, P. G. Radaelli, H. N. Bordallo, and D. E. Cox, Phys. Rev. B **59**, 8695 (1999).

[29] M. Kubota, H. Fujioka, K. Ohoyama, K. Hirota, Y. Moritomo, H. Yoshizawa, and Y. Endoh, J. Phys. Chem. Solids **60**, 1161 (1999).

[30] M. Kubota, H. Fujioka, K. Hirota, K. Ohoyama, Y. Moritomo, H. Yoshizawa, and Y. Endoh, J. Phys. Soc. Jpn. **69**, 1606 (2000).

[31] R. M. Kusters, J. Singleton, and D. A. Keen, Physica B **155**, 362 (1989).

[32] G. J. Snyder, R. Hiskes, S. DiCarolis, M. R. Beasley, and T. H. Geballe, Phys. Rev. B **53**, 14 434 (1996).

[33] M. Viret, L. Ranno, and J. M. D. Coey, Phys. Rev. B **55**, 8067 (1997).

[34] H. Fritzsche, Solid State Commun. **9**, 1813 (1971).

[35] N. F. Mott and E. A. Davis, *Electronic Processes in Non-Crystalline Materials*, 2nd ed. (Clarendon Press, Oxford, 1979).

[36] Nevill Mott, *Conduction in Non-Crystalline Materials* (Clarendon Press, Oxford, 1993).

[37] J. M. D. Coey, M. Viret, L. Ranno, and K. Ounadjela, Phys. Rev. Lett. **75**, 3910 (1995).